The bending of single layer graphene sheets: the lattice versus continuum approach

F Scarpa[1], S Adhikari[2], A J Gil[2] and C Remillat[3]

[1] Advanced Composites Centre for Innovation and Science, University of Bristol, Bristol BS8 1TR, UK
[2] School of Engineering, Swansea University, Singleton Park, Swansea SA2 8PP, UK
[3] Aerospace Engineering, University of Bristol, BS8 1TR, UK

E-mail: f.scarpa@bris.ac.uk, S.Adhikari@swansea.ac.uk and A.J.Gil@swansea.ac.uk

Abstract
The out-of-plane bending behaviour of single layer graphene sheets (SLGSs) is investigated using a special equivalent atomistic-continuum model, where the C–C bonds are represented by deep shear bending and axial stretching beams and the graphene properties by a homogenization approach. SLGS models represented by circular and rectangular plates are subjected to linear and nonlinear geometric point loading, similar to what is induced by an atomic force microscope (AFM) tip. The graphene models are developed using both a lattice and a continuum finite element discretization of the partial differential equations describing the mechanics of the graphene. The minimization of the potential energy allows us to identify the thickness, elastic parameters and force/displacement histories of the plates, in good agreement with other molecular dynamic (MD) and experimental results. We note a substantial equivalence of the linear elastic mechanical properties exhibited by circular and rectangular sheets, while some differences in the nonlinear geometric elastic regime for the two geometrical configurations are observed. Enhanced flexibility of SLGSs is observed by comparing the nondimensional force versus displacement relations derived in this work and the analogous ones related to equivalent plates with conventional isotropic materials.

(Some figures in this article are in colour only in the electronic version)

1. Introduction

Single layer graphene sheets (SLGSs) are one atom thick two-dimensional layers of sp^2-bonded carbon densely packed to form a honeycomb crystal lattice. The graphene Young's modulus and thermal conductivity rival the analogous properties of graphite (1.06 TPa and 3000 W m^{-1} K^{-1} respectively) [1, 2]. The enhanced flexibility of graphene sheets, despite their high Young's modulus, has been attributed to the change in curvature given by reversible elongation of sp^2 C–C bonds [3], showing also the presence of ripples over the surface [4] and the possibility of multiple folding when embedded in a coarse grain [5]. These unusual mechanical characteristics, coupled with the multifunctional properties, make graphene sheets an excellent platform to design a novel class of advanced composites and nanosensors with superior mechanical and electric performance [6–10].

The graphene (and graphite) models proposed in the literature were initially based on interactions provided by axial and rotational springs on an hexagonal lattice [11]. There are analytical approaches based on low-energy continuum mechanics approaches (see e.g. [12] and references therein). Such approaches, albeit perhaps less accurate, can provide physical intuition. MD and models based on Tersoff–Brenner potentials [13], as well as the Cauchy–Born rule [14], have also been proposed and their results mainly benchmarked against available data from other simulations, or bulk graphite properties. Recently, experimental data on the out-of-plane properties of graphene have been made available on multilayer [15] and SLGSs loaded with AFM

tips [16]. Specific out-of-plane SLGS simulations have been carried out using a meshless approach [17] and continuum mechanics representations based on MD force models [18, 19], while the flexural behaviour of SLGS has been modelled in resonance mode using truss-like structural assemblies [20]. The theoretical mechanical properties provide a broad agreement over the tensile rigidity of SLGS between 0.190 and 0.350 TPa nm, according to the size and loading conditions of the graphene samples [21]. However, a significant scattering is observed for the thickness values of the graphene, similarly to single wall carbon nanotubes (the 'Yakobson's Paradox' [22]). To solve the problem, the thickness of the SLGS (and carbon nanotubes (CNTs)) is generally assumed equal to 0.34 nm, the interlayer graphite atomic distance. In this work, we make the distinction between the pure geometric definition of thickness and its representation in continuum mechanics. We use the concept of thickness to adopt an equivalent continuum model representing the mechanical behaviour of the nanocomponent. In SLGSs, as in single wall carbon nanotubes, the thickness of the equivalent continuum (say a plate or a hollow tube) should be equal to that of the C–C bonds composing the nanostructures. However, there is neither any physical thickness *per se* for the covalent bonds, nor for the carbon atoms involved. Nonetheless, the nanostructure subjected to a mechanical static loading tends to reach its equilibrium state corresponding to the minimum potential energy. The geometric and material configuration of the equivalent continuum mechanics structures (plate and/or hollow tube) will be therefore defined by the energy equilibrium conditions of the nanostructure, and cannot be ascribed as fixed. The length of the covalent bonds also merits some consideration. In finite size rectangular SLGSs, the lengths of the C–C bonds at equilibrium after loading are unequal, ranging between 0.136 and 0.144 nm, and depend on the type of loading, size and boundary conditions of the mechanical case [14, 23] and the location of the SLGS itself (i.e. the edges [24]). This fact contrasts with the classical use of the fixed value of 0.142 nm at equilibrium considered in most mechanical simulations [25, 20, 26, 27]. The variation of thickness and distributions of equilibrium length are important factors to consider when computing the *homogenized* mechanical properties of the graphene, i.e. the equivalent mechanical performance of the graphene as a *continuum*. Homogenization theory applied to periodic structures dictates a minimum number of periodic elements to identify asymptotic values for the linear elastic mechanical properties (stiffness, Poisson's ratios) [28, 29]. However, the variability of thickness and equilibrium lengths over the same graphene sheets when subjected to different loading conditions will result in different averaged homogenized mechanical properties according to the test cases. In that sense, the graphene behaves as a *structure*, not as an equivalent continuum material.

The authors have recently formulated a modelling approach, where the equivalent homogenized properties of the graphene sheets are expressed in terms of the thickness, equilibrium lengths and force models used to represent the C–C bonds of the graphene lattice [21]. The covalent bonds

are represented as structural beams with stretching, bending, torsional and deep shear deformation, based on the equivalence between the harmonic potential expressed in terms of the AMBER [30] or Morse models [31] and the mechanical strain energies associated with affine deformation mechanisms. The overall mechanical properties and geometric configurations of the graphene sheets and CNTs are then calculated, minimizing the total potential energy associated with models of nanostructures subjected to mechanical loading. The models are developed using finite element approaches, representing either the nanostructures as truss assemblies with the C–C bond equivalent beams or as having previously homogenized mechanical properties. These properties in turn are functions of the force model, thickness and average equilibrium length of the bonds. The nonlinear mechanical simulations are also carried out on circular and rectangular SLGSs with no prestress provided by external membrane tension (either mechanically applied or induced through thermal loading). The results illustrated are therefore only affected by the intrinsic elastic mechanical properties and nonlinear geometric deformation of the graphene plates.

2. Methodology

2.1. Lattice model

The carbon–carbon sp^2 bonds can be considered as equivalent beams having axial, out-of-plane and in-plane rotational deformation mechanisms. The harmonic potential associated with the C–C bond can be expressed as [27]:

$$U_r = \tfrac{1}{2}k_r(\delta r)^2 \qquad U_\theta = \tfrac{1}{2}k_\theta(\delta\theta)^2 \qquad U_\tau = \tfrac{1}{2}k_\tau(\delta\varphi)^2. \tag{1}$$

The equivalent mechanical properties of the C–C bond can be calculated using a beam mapping technique, imposing the equivalence between the harmonic potential and the mechanical strain energies of a hypothetical structural beam of length L [21]:

$$\frac{k_r}{2}(\delta r)^2 = \frac{EA}{2L}(\delta r)^2 \tag{2a}$$

$$\frac{k_\tau}{2}(\delta\varphi)^2 = \frac{GJ}{2L}(\delta\varphi)^2 \tag{2b}$$

$$\frac{k_\theta}{2}(\delta\theta)^2 = \frac{EI}{2L}\frac{4+\Phi}{1+\Phi}(\delta\theta)^2. \tag{2c}$$

Equation (2a) corresponds to the equivalence between the stretching and axial deformation mechanism (with E being the equivalent Young's modulus), while equation (2b) equates the torsional deformation of the C–C bond with the pure shear deflection of the structural beam associated with an equivalent shear modulus G. Contrary to similar approaches previously used [27, 20], the term equating the in-plane rotation of the C–C bond (equation (2c)) is equated to a bending strain energy related to a deep shear beam model, to take into account the shear deformation of the cross section. The shear correction term becomes necessary when considering beams with aspect
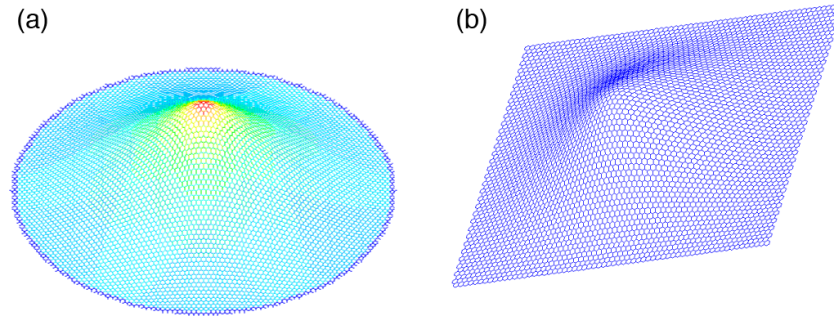
(a) (b)

Figure 1. Lattice models of circular and rectangular graphene sheets. The figures show a typical pattern of stress and deformation distribution under loading represented by a point force or distributed pressure over a small radius (such as those arising due an AFM tip). (a) Circular lattice plate ($R = 9.5$ nm) under central loading. Distribution of equivalent membrane stresses. (b) Deformation behaviour of a lattice rectangular SLGS plate ($a = 15.1$ nm, $b = 13.03$ nm) under central loading.

ratios lower than 10 [32]. For circular cross sections, the shear deformation constant can be expressed as [21]:

$$\Phi = \frac{12EI}{GA_s L^2}. \tag{3}$$

In equation (3), $A_s = A/F_s$ is the reduced cross section of the beam by the shear correction term F_s [33]:

$$F_s = \frac{6 + 12\nu + 6\nu^2}{7 + 12\nu + 4\nu^2}. \tag{4}$$

The insertion of (3) and (4) in (2) leads to an nonlinear relation between the thickness d and the Poisson's ratio ν of the equivalent beam [21]:

$$k_\theta = \frac{k_r d^2}{16} \frac{4A + B}{A + B} \tag{5}$$

where

$$A = 112L^2 k_\tau + 192L^2 k_\tau \nu + 64L^2 k_\tau \nu^2 \tag{6}$$
$$B = 9k_r d^2 + 18k_r d^4 \nu + 9k_r d^4 \nu^2. \tag{7}$$

The values for the force constants for the AMBER model are $k_r = 6.52 \times 10^{-7}$ N mm^{-1}, $k_\theta = 8.76 \times 10^{-10}$ N nm rad^{-2} and $k_\tau = 2.78 \times 10^{-10}$ N nm^{-1} rad^{-2}. For the linearized version of the Morse potential, we adopt $k_r = 8.74 \times 10^{-7}$ N mm^{-1}, $k_\theta = 9.00 \times 10^{-10}$ N nm rad^{-2} and $k_\tau = 2.78 \times 10^{-10}$ N nm^{-1} rad^{-2}. The equivalent mechanical properties of the C–C bond can be determined by performing a nonlinear optimization of equations (2a)–(2c) using a Marquardt algorithm [34]. The C–C bond can then be discretized as a single two-nodes three-dimensional finite element (FE) model beam with a stiffness matrix described in [35], where the nodes represent the atoms. The lattice models of the circular (figure 1(a)) and rectangular (figure 1(b)) graphene sheets are assembled using the FE discretization, with loading represented by a point force or distributed pressure over a small radius. Both for the linear elastic and nonlinear geometric elastic loading, at each substep of the Newton–Raphson solver technique [36] the total potential energy is minimized to identify the thickness of the C–C bonds and the average equilibrium length of the covalent bonds. The nonlinear minimization technique is performed in two steps, with a zero order method to identify first the minimal clusters, and a subsequent first order derivative based method to identify the absolute minimum of the potential energy.

2.2. Continuum model

In mechanical models for plates and shells, it is necessary to introduce a continuum homogeneous material, in the form of a Young's modulus and Poisson's ratio for isotropic mechanical configurations. The continuum homogenized properties of a single layer graphene sheet are calculated using an equivalent honeycomb approach (EMA) used by the authors in [21]. The unit cell of the SLGS is represented by beams with equivalent hinging, stretching, bending and shear stiffness calculated using the mechanical properties derived from the equivalence between the bonds' harmonic potential and the associated strain energies of a Timoshenko deep shear beam [21]. For the case of pure hinging–stretching (HS) deformation [37], the in-plane tensile rigidity Y (the product between the SLGS Young's modulus E and the thickness d) and the SLGS Poisson's ratio ν_g are expressed in the following manner:

$$Y = \frac{4\sqrt{3}k_r K_h}{3(k_r + 3K_h)} \tag{8}$$

$$\nu_g = \frac{1 - \frac{K_h}{k_r}}{1 + 3\frac{K_h}{k_r}}. \tag{9}$$

Here K_h is the equivalent hinging force constant for the C–C bond [21]. Equations (8) and (9) can be modified to consider other equivalent deformation mechanisms for the graphene C–C bonds, such as hinging–stretching–bending (HSB), and hinging–stretching–bending-deep shear (HSBD) [21].

The variational formulation for the equation of a circular plate in polar coordinates under central point loading undergoing membrane and nonlinear geometric bending can be expressed as [18, 38]:

$$\int_0^a \left[D\frac{d(\Delta w)}{dr} - \psi - \frac{1}{r}\frac{dF}{dr}\frac{dw}{dr} \right] \frac{d(\Delta w)}{dr} r\, dr = 0 \tag{10}$$

where

$$\psi = \frac{1}{r}\int_0^r qs\, ds. \tag{11}$$

In the above equations w is the out-of-plane deformation of the plate, q is the generalized load normal to the plane of the plate, and $\frac{d^2 F}{dr^2} = N_t$ and $\frac{1}{r}\frac{dF}{dr} = N_r$, where F is a
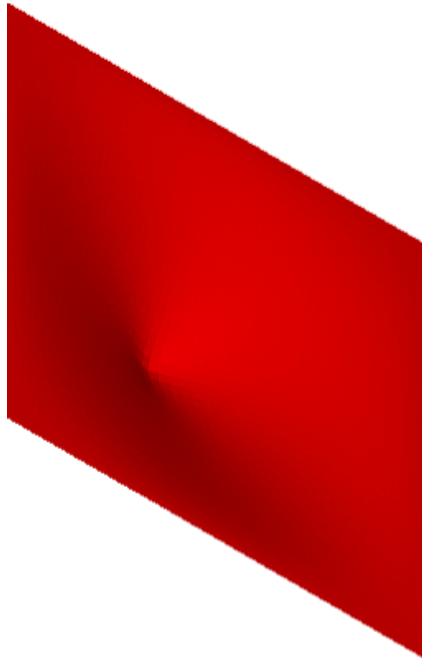
Figure 2. Continuum rectangular plate ($a = 15.1$ nm, $b = 13.03$ nm) under central loading. Distribution of the out-of-plane deformations.

Table 1. Equilibrium thickness, length and mechanical properties for circular lattice SLGSs under concentrated central loading. E is the Young's modulus, ν_g is the Poisson's ratio, l is the equilibrium bond length and Y is the in-plane tensile rigidity. The numbers of atoms used in the simulation are as follows: radius 2.5 nm (3843), radius 2.5 nm (6236), radius 2.5 nm (11 884).

Radius (nm)	d (nm)	E (TPa)	ν_g	l (nm)	Y (TPa nm)
Force model: Morse					
2.5	0.088	3.74	0.33	0.142	0.329
5.0	0.087	3.80	0.33	0.141	0.330
9.5	0.087	3.76	0.33	0.141	0.327
Force model: AMBER					
2.5	0.100	2.54	0.32	0.144	0.254
5.0	0.100	2.56	0.32	0.144	0.256
9.5	0.100	2.60	0.32	0.140	0.260

Table 2. Equilibrium thickness, length and mechanical properties for circular continuum SLGSs under concentrated central loading. E is the Young's modulus, ν_g is the Poisson's ratio, l is the equilibrium bond length and Y is the in-plane tensile rigidity.

Radius (nm)	d (nm)	E (TPa)	ν_g	l (nm)	Y (TPa nm)
Force model: Morse					
2.5	0.087	3.80	0.33	0.136	0.330
5.0	0.088	3.75	0.33	0.141	0.330
9.5	0.087	3.76	0.33	0.142	0.327
Force model: AMBER					
2.5	0.100	2.53	0.33	0.144	0.253
5.0	0.100	2.54	0.32	0.144	0.254
9.5	0.100	2.58	0.32	0.142	0.258

suitable stress function. Here N_t and N_r are, respectively, the membrane force per unit length along the tangential and radial directions. The flexural rigidity of the plate is $D = Yd^2/12(1 - \nu_g^2)$. The minimization of equation (10) is performed by discretizing the plate with axisymmetric finite elements with linear interpolation shape functions [39].

For a rectangular plate in Cartesian coordinates with membrane and nonlinear bending deformation, the von Karman equation for the potential energy can be expressed as [40]:

$$\Pi^* = \int\int\left\{-\frac{A_1}{2Y} + \frac{DA_2}{2} + \frac{A_3}{2} - \bar{p}w\right\}\mathrm{d}x\,\mathrm{d}y \quad (12)$$

where

$$A_1 = \left(\frac{\partial^2 F}{\partial x^2} + \frac{\partial^2 F}{\partial y^2}\right)^2 + 2(1 + \nu_g)\left(\left(\frac{\partial^2 F}{\partial x\partial y}\right)^2 - \frac{\partial^2 F}{\partial x^2}\frac{\partial^2 F}{\partial y^2}\right) \quad (13)$$

$$A_2 = \left(\frac{\partial^2 w}{\partial x^2} + \frac{\partial^2 w}{\partial y^2}\right)^2 + 2(1 - \nu_g)\left(\left(\frac{\partial^2 w}{\partial x\partial y}\right)^2 - \frac{\partial^2 w}{\partial x^2}\frac{\partial^2 w}{\partial y^2}\right) \quad (14)$$

$$A_3 = \frac{\partial^2 F}{\partial y^2}\left(\frac{\partial w}{\partial x}\right) + \frac{\partial^2 F}{\partial x^2}\left(\frac{\partial w}{\partial y}\right)^2 - 2\frac{\partial^2 F}{\partial x\partial y}\frac{\partial w}{\partial x}\frac{\partial w}{\partial y}. \quad (15)$$

In (12) $\bar{p}$ is the external distributed pressure, which can be changed into a point loading by use of the integral of a Dirac function [40, 18]. The functional F is expressed as:

$$\Delta^2 F = Y\left[\left(\frac{\partial w^2}{\partial x\partial y}\right)^2 - \frac{\partial w^2}{\partial x^2}\frac{\partial^2 w}{\partial y^2}\right] \quad (16)$$

where Δ^2 is the Laplace operator. For the rectangular model, a FE discretization can be performed using general conformal mapping rectangular elements [41].

The lattice and continuum SLGS models were loaded with a concentrated central force having a maximum magnitude of 500 nN. Both for the circular and rectangular SLGSs (figure 2), the minimization of the potential energy during the static loading is performed using the same nonlinear minimization technique used for the lattice model.

3. Results

3.1. Circular graphene sheets

Tables 1 and 2 show the values for the thickness and mechanical properties for a circular graphene sheet modelled with the lattice and continuum approaches, respectively. The homogenized Young's modulus and Poisson's ratio have been calculated using equations (8) and (9), considering a stretching–hinging deformation mechanism for the C–C bond [21]. For both approaches we observe a remarkable consistency between the mechanical properties predicted with the same force model. The linearized Morse potential provides average thickness values $d \sim 0.088$ nm, and equilibrium lengths varying between 0.136 and 0.142 nm. For the AMBER case, both the lattice and continuum approach provide an equilibrium value of the thickness $d = 0.100$ nm and average equilibrium lengths ranging between 0.140 and 0.144 nm. The homogenized Young's modulus of the SLGS is significantly

dependent on the force model used and, to a certain extent, on the radius of the graphene sheet itself. For all cases, the Young's modulus is on average 30% lower when the AMBER force model is used, due to its lower stretching force constant. It is worth noticing that the equivalent Young's modulus identified for the 9.5 nm radius SLGS is 3.76 TPa, both for the continuum and lattice approaches; however, the Young's modulus shows a discrepancy of around 1% when considering lower SLGS radii (2.5 and 5 nm). The dependence of the equivalent continuum mechanical properties of a cellular structure over the number of its periodic units is an aspect considered in classical mechanical homogenization theory and large numbers of unit cells are required to approximate the asymptotic values. It is remarkable, however, that the Poisson's ratio is constant for all the Morse potential configurations at 0.33. Similar considerations for the distributions of mechanical properties are valid also for the case of the AMBER force model, where the Young's modulus is identified as being equal to 2.60 TPa for $R = 9.5$ nm and the Poisson's ratio ν_{xy} is constant for all configurations at 0.32. The tensile rigidity Y varies with the force model used, with an average of 0.255 and 0.257 TPa nm for the AMBER SLGS represented by the continuum and lattice models, respectively. A stiffening effect is observed for the Morse potential cases, with an average tensile rigidity of 0.329 TPa nm, both for the continuum and lattice models.

The values of average length, thickness and mechanical properties are in good agreement with the analogous values present in the available literature. Both for the continuum and lattice models, the equilibrium lengths are on average around 0.144 nm, slightly higher than the classical 0.142 nm indicated for C–C bonds [42, 43]. For the circular SLGS continuum Morse model with a radius of 2.5 nm (table 2) the equilibrium length is 0.136 nm, a value that is close to the one encountered in nanostructures with Stone–Walls defects [1]. Variation of equilibrium lengths in SLGSs has been observed by Reddy *et al* using the Cauchy–Borne rule [14] and in [21] for the case of in-plane mechanical tensile and shear loading. The so-called 'Yakobson's paradox' [22] for the thickness and axial Young's modulus in CNTs is well present also for graphene nanostructures. For the in-plane loading of SLGS nanostructures, the thickness d varies from 0.057 nm [44] to 0.335 nm [45]. Tu and Ou-Yang [46] determined a thickness of 0.074 nm, while Kudin *et al* [47] identified a value of 0.084 nm, very close to the 0.087 nm from the Morse potential of this work. Scarpa *et al* [21] observed thickness values between 0.074 and 0.084 nm, depending on the deformation mechanism assumed for the SLGS. However, all the cited values are referred to in-plane loading of the graphene sheets. For out-of-plane loading, Sakhaee-Pour [26] imposed a thickness of 0.34 nm equal to the atomic interlayer distance between graphene layers in bulk graphite. The same thickness is assumed for the experimental results on bi-layer graphene of Frank *et al* [15] and Lee *et al* [16]. Hemmasizadeh *et al* identified a thickness of 0.137 nm [18], close to the 0.12 nm of Sun *et al* in CNTs [43], slightly higher compared to our AMBER models (0.100 nm). Duan and Wang [19] derive a value $d = 0.052$ nm for a circular SLGS of 4 nm

diameter, imposing a Poisson's ratio equal to 0.16. The latter ν_g value is equal to the one from [42, 48] and close to the 0.15 of Kudin *et al* [47]. Our models, both continuum and lattice, predict constant Poisson's ratios between 0.32 and 0.33, which are consistent with the results from second generation Tersoff–Brenner potentials ($\nu_g = 0.39$ [44]) and from the continuum limit of the local density formulation ($\nu_g = 0.34$ [46]). The tensile rigidity from our models based on the AMBER force field (~256 TPa nm) bears a good agreement with the $Y = 0.243$ TPa nm from [44], 277 TPa nm of Caillerie *et al* [37] and 0.251 TPa nm from the harmonic average of the orthotropic in-plane stiffness of Reddy *et al* [14]. The average tensile rigidity from the Morse potential used in our models (average 0.329 TPa nm) is similar to the 0.349 TPa nm from [47] and the 0.337–0.354 TPa nm of Sakhaee-Pour *et al* [25]. Concerning the tensile rigidity from out-plane (bending) loading, Duan and Wang [19] determined a value of 0.358 TPa nm, while the experimental single point loading of Lee *et al* showed a tensile rigidity of 0.342 TPa nm [16]. We have reproduced the experimental case related to the SLGS (radius 1200 nm) under central point loading [16], using the continuum finite element approach with the linearized Morse potential and our simulations provide a tensile rigidity $Y = 0.333$ TPa nm, 2.6% lower than the one from the experimental measurement.

The nondimensional force versus displacement for a circular SLGS under central loading is described by Hemmasizadeh *et al* as [18]:

$$\frac{\bar{F}R^2}{Yd^3} = \frac{4.2017}{1 - \nu_g^2}\frac{w}{d} + 2.0462\left(\frac{w}{d}\right)^3 \qquad (17)$$

where $\bar{F}$ is the point load and R the radius of the graphene sheet. The linear part ($\frac{w}{d}$) of equation (17) corresponds to the nondimensional flexural stiffness, while the cubic dependence on the displacement/thickness ratio is proportional to the membrane stiffness of the equivalent continuum material. The $(w/d)^3$ behaviour if the out-of-plane stiffness of SLGSs has also been observed experimentally by [16, 15]. Equation (17) has been rewritten to take into account that the diaphragm stresses are only due to the elasticity of the graphene sheet, and have a form of the type $K_1/(1 - \nu_g^2)$, while the nondimensional bending stiffness has a constant of proportionality K_2 versus $(w/d)^3$ [49]. In a dimensional form, the mismatch between equation (17) and the force–deflection curve obtained by Medyanik [17] is around 1%.

A comparison between equation (17) and the continuum and lattice models (Morse potential) for different radii is presented in figure 3. There is a very good agreement between the analytical formula (17) and the lattice representations for the different radii. The continuum models also show a very satisfactory agreement for radii up to 5.0 nm, all featuring a slight strain softening effect compared to the lattice models, with the exception of the SLGS with $R = 9.5$ nm, where this effect is more significant. The constant 4.2017 in equation (17) is similar to the value $K_1 = 5.33$ for isotropic plates with clamped edges, but with no tension held and subjected to a uniform pressure distribution [49]. The constant 2.0462 is also close to the value $K_2 = 3.44$ related to a plate with
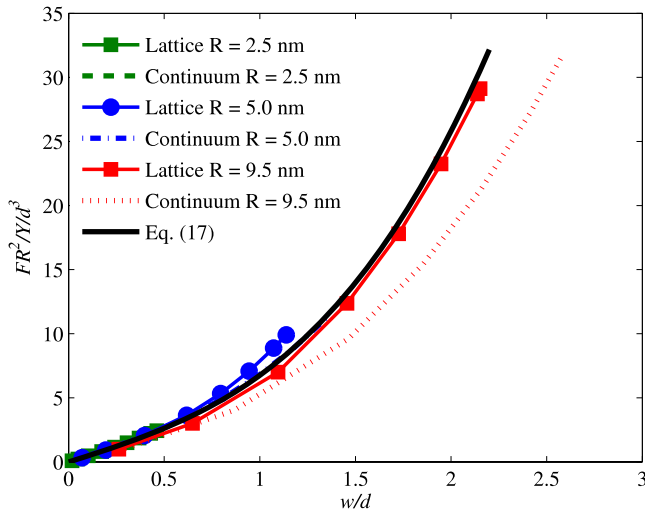
Figure 3. Comparison of the nondimensional force versus nondimensional out-of-plane displacement for circular lattice and continuum SLGSs.

Table 3. Equilibrium thickness, length and mechanical properties for rectangular continuum SLGSs.

Dimensions $a \times b$ (nm $\times$ nm)	d (nm)	E (TPa)	ν_g	l (nm)	Y (TPa nm)
Force model: Morse					
4.14 × 3.55	0.080	3.75	0.33	0.144	0.300
7.66 × 6.55	0.086	3.92	0.42	0.140	0.337
15.1 × 13.03	0.084	4.06	0.37	0.142	0.340
Force model: AMBER					
4.14 × 3.55	0.100	2.57	0.32	0.144	0.257
7.66 × 6.55	0.100	2.55	0.32	0.142	0.255
15.1 × 13.03	0.100	2.68	0.31	0.136	0.268

pure diaphragm stiffness and $K_2 = 2.89$ for a circular plate fixed and held. It must be noticed that for loading conditions approaching the concentrated load, the values K_1 and K_2 change significantly, with K_1 assuming values higher than 27 and K_2 of 14. These results can be considered a further demonstration of the enhanced flexibility of SLGSs under out-of-plane loading, with their nondimensional stiffness similar to the one provided by an equivalent isotropic plate under uniform pressure, rather than point loading.

3.2. Rectangular graphene sheets

The rectangular SLGSs under out-of-plane loading show an overall similar trend to the circular graphene plates, although some specific differences can be observed.

Rectangular SLGSs show an in-plane special orthotropic behaviour [50, 14, 51, 21], following the reciprocity relationships for special orthotropic materials: $E_x \nu_{yx} = E_y \nu_{xy}$, which is typical of cellular and honeycomb structures [52]. As a normalizing metric, the equivalent mechanical properties of a general anisotropic medium can be represented by their geometric average [53]. In this context, the equivalent homogenized properties identified during the out-of-plane

Table 4. Equilibrium thickness, length and mechanical properties for rectangular lattice SLGSs. The numbers of atoms used in the simulation are as follows: dimension 4.14 × 3.55 nm^2 (2176), dimension 7.66 × 6.55 nm^2 (4228), dimension 15.1 × 13.03 nm^2 (8448).

Dimensions $a \times b$ (nm $\times$ nm)	d (nm)	E (TPa)	ν_g	l (nm)	Y (TPa nm)
Force model: Morse					
4.14 × 3.55	0.088	3.74	0.33	0.142	0.329
7.66 × 6.55	0.088	3.75	0.33	0.141	0.330
15.1 × 13.03	0.087	3.76	0.33	0.136	0.327
Force model: AMBER					
4.14 × 3.55	0.122	1.83	0.54	0.144	0.223
7.66 × 6.55	0.123	1.80	0.54	0.135	0.221
15.1 × 13.03	0.124	1.80	0.54	0.136	0.223

bending loading in tables 3 and 4 can be represented as $E = \sqrt{E_x E_y}$ and $\nu_g = \sqrt{\nu_{xy} \nu_{yx}}$. For an isotropic material in two dimensions, the Poisson's ratio is limited between −1 and +1. Special orthotropic materials do obey only the reciprocity relation and therefore their Poisson's ratios ν_{xy} or ν_{yx} could have values outside the isotropic bounds [52].

The continuum Morse force field model (table 3) provides equilibrium lengths varying between 0.140 and 0.144 nm, while the simulations related to the AMBER case show a drop of the average L up to 0.136 nm. The distribution of the equilibrium lengths is substantially unchanged for the lattice case (table 4); however, the various L for the AMBER cases are on average lower than the continuum representation (∼0.138 nm). For the linearized Morse potential in the lattice case, the average thickness is around 0.088 nm, with no evident relation to the dimensions of the SLGS. The AMBER cases show a higher average bond thickness for the lattice representation ($d = 0.123$ nm) and a slightly lower one for the continuum model ($d = 0.100$ nm). The continuum case shows average thickness values of 0.083 nm for the linearized Morse potential, 6% lower than the ones provided by the lattice case. Quite significantly, the Young's modulus identified with equation (8), using the values of thickness and length after the minimization of the total potential energy, is in general stiffer for the continuum model than for the lattice one. As an example, the largest rectangular graphene sheet simulated in this work (15.1 nm × 13.03 nm—see figures 1(b) and 2) shows Young's moduli of 4.06 TPa and 3.76 TPa for the continuum and lattice cases, respectively. Similar high values of the in-plane Young's modulus have been found in SLGSs under tension using first generation (3.81 TPa) and second generation (4.23 TPa) Tersoff–Brenner potentials [44]. Similarly to the circular SLGS case, the AMBER based Young's modulus is significantly lower than in the Morse potential case (average 2.60 TPa for the three configurations)—again, due to the lower stretching constant force. When considering the lattice models, the ones based on the linearized Morse potential provide a good agreement with the continuum ones, while the AMBER based finite element representations show a significant lowering of the identified Young's modulus from equation (8), with an average $E_g = 1.82$ TPa. Albeit lower than the Morse based

ones, the values of the Young's modulus calculated with the AMBER force model are in line with the ones from [48, 45] (1.15 TPa) and [42] (1.06 TPa). A Young's modulus close to 1.80 TPa was observed by Scarpa *et al* in combined HSB dominated deformations due to in-plane loading [21]. The Poisson's ratio ν_g for the continuum Morse case varies between 0.33 and 0.42, again in line with predictions from Huang *et al* (0.41 for the second generation TB potential) [44]. The Morse lattice simulations are also in line with the continuum ones, with an average $\nu_g = 0.33$. The situation is different for the AMBER force field, where the continuum models predict a geometric averaged Poisson's ratio of 0.32, while the lattice ones provide $\nu_g = 0.54$. The reason for the discrepancy between the two models lies in the difference between average equilibrium lengths and, more importantly, between bond thicknesses (0.123 nm for the lattice, 0.100 nm for the continuum). The different thicknesses affect the hinging constant $K_h = 8k_\tau/d^2$ [21], which affects the in-plane mechanical properties ((8) and (9)). The average Poisson's ratio of 0.54 for the AMBER lattice model is comparable with the values from [14] (0.47) and [21] (0.51). We report also the value of 1.27 simulated by Sakhaee-Pour [26], a Poisson's ratio which could be partly explained if the C–C bonds behave under pure flexural and deep shear deformation, like in thick honeycombs [21]. However, it must emphasized that all the cited results are related to SLGSs loaded in-plane, while the results from our models are referred to pure out-of-plane bending loading. The homogenized in-plane rigidity Y for the Morse potential is substantially equivalent for the lattice and continuum models (average 0.329 TPa nm and 0.326 TPa nm respectively). One can notice that for the continuum model, both the Young's modulus and tensile rigidity increase asymptotically with the size of the SLGS, a feature typical of mechanical homogenization processes [29]. The tensile rigidity values are in very good agreement with the ones related to the circular graphene sheets described in this work and elsewhere in the literature. For the AMBER force field, comparable tensile stiffnesses under in-plane tensile loading for rectangular graphene can be found in the works of Caillerie *et al* [37] (0.277 TPa nm), Reddy *et al* [14] and Huang *et al* [44].

Using the perturbation approach of [18] applied to equation (16), one could obtain a relation between the nondimensional force and the normalized out-of-plane displacement similar to equation (17):

$$\frac{\bar{F}ab}{Yd^3} = \frac{4.541}{1-\nu_g^2}\frac{w}{d} + 1.365\left(\frac{w}{d}\right)^3 \qquad (18)$$

where a and b are, respectively, the major and minor dimensions of the rectangular SLGS and ν_g has to be considered the geometric average of the in-plane Poisson's ratios. One can notice the similarity in terms of magnitude of the linear term of equation (18) compared to the analogous one of the circular SLGSs in equation (17). The nondimensional membrane stiffness (cubic part) is, however, 64% of the analogous one for the circular graphene sheet, suggesting that membrane-induced deformations dominate in rectangular SLGSs unlike in their circular counterpart.
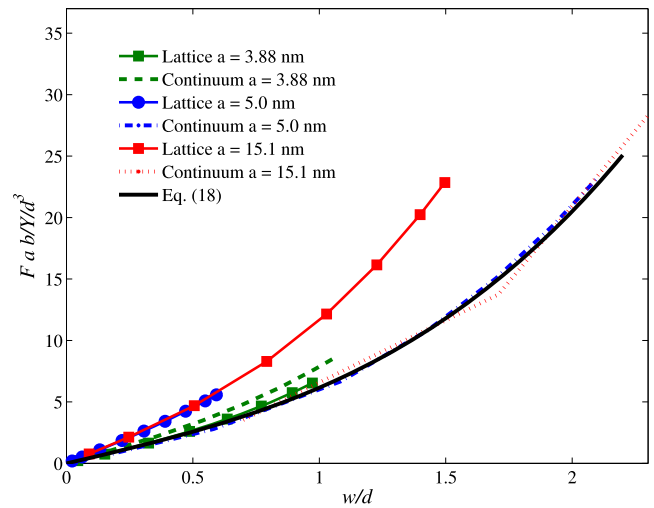

Figure 4. Comparison of the nondimensional force versus nondimensional out-of-plane displacement for rectangular lattice and continuum SLGSs. The aspect ratio for the plates is 1.15:1.

Figure 4 shows a comparison between the nondimensional point loading using the continuum, lattice and equation (18) approaches. Similarly to the circular graphene case, there is a close agreement between the continuum model solved with finite shell elements and the analytical formula. Lattice models with lower dimensions also follow equation (18) quite satisfactorily. However, the two rectangular lattice SLGS configurations ($a = 5.0$ and 15.1 nm) show a stiffening effect compared to the continuum finite element formulations and equation (18). We have observed that the continuum model with conformal mapping elements (figure 2) provides combined membrane and bending maximum stresses close to 35% less than the lattice model (figure 1(b)), which is composed of Timoshenko beams. This fact seems to suggest that the lattice model is more sensitive to the stiffening effect provided by the presence of corners in the rectangular cellular structure representing the graphene and shows a lower decay of the membrane Saint-Venant's effects of the edges [54].

It is interesting to compare the nondimensional force versus displacement of equation (4) and the analogous for an equivalent clamped isotropic rectangular plate, as available in the literature, which is given by the relation [49]:

$$\frac{qa^2}{Yd^3} \sim 19.3\left(\frac{w}{d}\right) + 38.41\left(\frac{w}{d}\right)^3. \qquad (19)$$

Equation (19) indicates that a rectangular plate fixed and held at the edges has a higher nondimensional stiffness (both bending and membrane) compared to a circular plate (see the coefficients K_2 and K_1 for the circular case of the previous paragraph). Even considering the stiffening effect given in the rectangular SLGS lattice case, the rectangular graphene sheet shows an out-of-plane stiffness similar to the circular topology, with the linear and cubic terms, respectively, 5 and 30 times lower than the ones of an equivalent plate made with classic isotropic material ($\nu = 0.31$ [49]).

4. Conclusions

Out-of-plane deformation of circular and rectangular SLGSs is considered in this study. Using the proposed methodology, it is possible to identify the equilibrium lengths and effective thickness of the circular and rectangular SLGSs corresponding to the minimum of the potential energy associated with out-of-plane mechanical nonlinear point loading. The predicted membrane and bending deformations of circular graphene sheets compare well with existing numerical and experimental results, while the tensile rigidity and overall deformation mechanism of rectangular SLGSs is consistent with that of circular graphene plates.

The main novelty of the work lies in the comparative analysis of the out-of-plane deformation of circular and rectangular graphene sheets and the provision of the predictive formulae to assess their transverse mechanical behaviour under point loading. While circular SLGSs have been considered in the past, to the best of our knowledge the nonlinear out-of-plane behaviour of rectangular graphene (excluding the ripple effects) is described here for the first time. We also gave further evidence of the increased flexibility of the graphene, comparing the nonlinear loading against known nondimensional stiffness equations related to isotropic conventional materials. The key conclusions arising from the analytical and numerical works reported in the paper are as follows.

 (i) The SLGSs under out-of-plane deformation assume different equivalent thicknesses and average equilibrium lengths compared to the in-plane cases listed in the available literature, although within the available range of the corresponding values for graphene and nanotubes. The minimization of the total potential energy seems therefore to confirm [44] that different thickness values have to be considered for specific mechanical loading.

 (ii) A rectangular SLGS under out-of-plane deformation assumes a tensile rigidity close to that identified in circular SLGSs, while the nondimensional membrane stiffness provided by the continuum and perturbation technique shows a slight softening effect compared to the circular case. Lattice models tend, however, to be stiffer, with higher bending stresses compared to the continuum cases.

(iii) Both the circular and rectangular graphene sheets show a lower nondimensional stiffness compared to analogous plates mechanically loaded and made with an equivalent isotropic material with constant ν, a further demonstration of the intrinsic enhanced flexibility of this particular nanostructure.

Acknowledgments

References

[1] Duplock E J, Scheffler M and Lindan P J D 2004 Hallmark of perfect graphene *Phys. Rev. Lett.* **92** 225502
[2] Novoselov K S, Geim A K, Morozov S V, Jiang D, Katsnelson M I, Grigorieva I V, Dubonos S V and Firsov A A 2005 Two-dimensional gas of massless Dirac fermions in graphene *Nature* **438** 197–200
[3] Couturier G, Aimé J P, Salardenne J, Boisgard R, Gourdon A and Gauthierl S 2001 A mechanical approach to the dissipation process in NC-AFM: experiments, model and simulation *Appl. Phys.* A **72** S47–50
[4] Bao W, Miao F, Chen Z, Zhang H, Jang W, Dames C and Lau C N 2009 Controlled ripple texturing of suspended graphene and ultrathin graphite membranes *Nat. Nanotechnol.* **4** 562
[5] Cranford S, Dipanjan S and Buehler M J 2009 Meso-origami: folding multilayer graphene sheets *Appl. Phys. Lett.* **95** 1231121
[6] Geim A K and Novoselov K S 2007 The rise of graphene *Nat. Mater.* **6** 183–91
[7] Katsnelson M I and Novoselov K S 2007 Graphene: new bridge between condensed matter physics and quantum electrodynamics *Solid State Commun.* **143** 3–13
[8] Stankovich S *et al* 2006 Graphene-based composite materials *Nature* **442** 202–6
[9] Brumfiel G 2009 Graphene gets ready for the big time *Nature* **458** 390–1
[10] Van Noorden R 2006 Moving towards a graphene world *Nature* **442** 228–9
[11] Gillis P P 1984 Calculating the elastic constants of graphite *Carbon* **22** 387
[12] De Martino A, Egger R and Gogolin A O 2009 Phonon–phonon interactions and phonon damping in carbon nanotubes *Phys. Rev.* B **79** 205408
[13] Brenner D W 1990 Empirical potential for hydrocarbons for use in simulating the chemicalvapor deposition of diamond films *Phys. Rev.* B **42** 9458–71
[14] Reddy C D, Rajendran S and Liew K M 2006 Equilibrium configuration and elastic properties of finite graphene *Nanotechnology* **17** 864
[15] Frank I W, Tanenbaum D M, van der Zande A M and LMcEuenm P 2007 Mechanical properties of suspended graphene sheets *J. Vac. Sci. Technol.* B **25** 2558–61
[16] Lee C, Wei X, Kysar J W and Hone J 2008 Measurement of the elastic properties and intrinsic strength of monolayer graphene *Science* **321** 385–8
[17] Medyanik S N, Karpov E G and Liu W K 2006 Domain reduction method for atomistic simulations *J. Comput. Phys.* **218** 836–59
[18] Hemmasizadeh A, Mahzoon M and Hadi E 2008 A method for developing the equivalent continuum model of a single layer graphene sheet *Thin Solids Films* **416** 7636
[19] Duan W H and Wang C M 2009 Nonlinear bending and stretching of a circular graphene sheet under a central point load *Nanotechnology* **20** 075702
[20] Sakhaee-Pour A, Ahmadian M T and Naghdabadi R 2008 Vibrational analysis of single-layered graphene sheets *Nanotechnology* **19** 085702
[21] Scarpa F, Adhikari S and Phani A S 2009 Effective elastic mechanical properties of single layer graphene sheets *Nanotechnology* **20** 065709
[22] Shenderova O A, Zhirnov V V and Brenner D W 2002 Carbon materials and nanostructures *Crit. Rev. Solid State Mater. Sci.* **27** 227
[23] Reddy C D, Ramasubramaniam A, Shenoy V B and Zhang Y W 2009 Edge elastic properties of defect-free single-layer graphene sheets *Appl. Phys. Lett.* **94** 101904
[24] Sun C Q, Sun Y, Nie Y G, Wang Y, Pan J S, Ouyang G, Pan L K and Sun Z 2009 Coordination-resolved C–C bond length and the C1s binding energy of carbon allotropes and the effective atomic coordination of the few-layer graphene *J. Phys. Chem.* C **113** 16464

[25] Sakhaee-Pour A, Ahmadian M T and Vafai A 2008 Potential application of single-layered graphene sheet as strainsensor *Solid State Commun.* **147** 336–40

[26] Sakhaee-Pour A 2009 Elastic properties of single-layered graphene sheet *Solid State Commun.* **149** 91

[27] Tserpes K I and Papanikos P 2005 Finite element modelling of single-walled carbon nanotubes *Composites* B **36** 468

[28] Ponte Castaneda P and Willis J R 1995 The effect of spatial distribution on the effective behavior of composite materials and cracked media *J. Mech. Phys. Solids* **43** 1919

[29] Bornert M, Bretheau T and Gilormini P 2008 *Homogenization in Mechanics of Materials* (London: Wiley-Iste)

[30] Cornell W D *et al* 1995 A second generation force field for the simulation of proteins, nucleic acids, and organic molecule *J. Am. Chem. Soc.* **117** 5179

[31] Belytschko T, Xiao S P and Ruoff R S 2002 Atomistic simulations for nanotube fracture *Phys. Rev.* B **65** 235430

[32] Timoshenko S 1940 *Theory of Plates and Shells* (London: McGraw-Hill)

[33] Kaneko T 1974 On Timoshenko's correction for shear in vibrating beams *J. Phys. D: Appl. Phys.* **8** 1927

[34] Marquardt D 1963 An algorithm for least-squares estimation of nonlinear parameters *J. Soc. Indust. Appl. Math.* **11** 431–41

[35] Przemienicki J S 1968 *Theory of Matrix Structural Analysis* (New York: McGraw-Hill)

[36] Bathe K J and Wilson E L 1976 *Numerical Methods in Finite Element Analysis* (Englewood Cliffs, NJ: Prentice-Hall)

[37] Caillerie D, Mourat A and Raoult A 2006 Discrete homogenization in graphene sheet modeling *J. Elasticity* **84** 33

[38] Timoshenko S 1940 *Theory of Plates and Shells* (New York: McGraw-Hill)

[39] Zienkiewicz O C, Bauer J, Morgan K and Onate E 1977 A simple and efficient element for axisymmetric shells *Int. J. Numer. Methods Eng.* **11** 1545–58

[40] Washizu K 1982 *Variational Methods in Elasticity and Plasticity* (Oxford: Pergamon)

[41] Deak A L and Pian T H H 1967 Application of the smooth surface interpolation to the finite element analysis *AIAA J.* **5** 187–9

[42] Chang T and Gao H 2003 Size-dependent elastic properties of a single walled carbon nanotube via a molecular mechanics model *J. Mech. Phys. Solids* **51** 1059

[43] Sun C Q, Bai H L, Tai B K, Li S and Jiang E Y 2003 Dimension, strength, and chemical and thermal stability of a single C–C bond in carbon nanotubes *J. Phys. Chem.* B **107** 7544

[44] Huang Y, Wu J and Hwang K C 2006 Thickness of graphene and single wall carbon nanotubes *Phys. Rev.* B **74** 245413

[45] Cho J, Luo J J and Daniel I M 2007 Mechanical characterization of graphite/epoxy nanocomposites by multi-scale analysis *Compos. Sci. Technol.* **67** 2399

[46] Tu Z and Ou-Yang Z 2002 Single-walled and multi-walled carbon nanotubes viewed as elastic tubes with the effective Young's moduli dependent on layer number *Phys. Rev.* B **65** 233407

[47] Kudin K N, Scuseria G E and Yakobson B I 2001 C2F, BN and C nanoshell elasticity from *ab initio* computations *Phys. Rev.* B **64** 235406

[48] Blakslee O L *et al* 1970 Elastic constants of compression-annealed pyrolitic graphite *J. Appl. Phys.* **44** 3373

[49] Young W C and Budynas R G 2002 *Roark's Formulas for Stresses and Strains* 7th edn (London: McGraw-Hill)

[50] Reddy C D, Rajendran S and Liew K M 2005 Equivalent continuum modeling of graphene sheets *Int. J. Nanosci.* **4** 631

[51] Rajendran S and Reddy C D 2006 Determination of elastic properties of graphene and carbon-nanotubes using Brenner potential: the maximum attainable numerical precision *J. Comput. Theor. Nanosci.* **3** 382–90

[52] Gibson L J and Ashby M F 1997 *Cellular Solids: Structure and Properties* 2nd edn (Cambridge: Cambridge University Press)

[53] Mainprice M and Humbert M 1994 Methods of calculating petrophysical properties from lattice preferred orientation data *Surv. Geophys.* **15** 575

[54] Horgan C O 1989 Recent developments concerning Saint Venant's principle: an update *Appl. Mech. Rev.* **42** 295